Monthly Notices
of the
ROYAL ASTRONOMICAL SOCIETY

MNRAS **469,** S20–S28 (2017)
Advance Access publication 2017 April 8

doi:10.1093/mnras/stx866

Seasonal changes of the volatile density in the coma and on the surface of comet 67P/Churyumov–Gerasimenko

Tobias Kramer,[1,2]★ Matthias Läuter,[1] Martin Rubin[3] and Kathrin Altwegg[3]

[1]*Zuse Institute Berlin, D-14195 Berlin, Germany*
[2]*Department of Physics, Harvard University, Cambridge, MA 02138, USA*
[3]*Space Research and Planetary Sciences, University of Bern, CH-3012 Bern, Switzerland*

Accepted 2017 April 5. Received 2017 April 3; in original form 2017 February 17

ABSTRACT

Starting from several monthly data sets of *Rosetta*'s COmetary Pressure Sensor, we reconstruct the gas density in the coma around comet 67P/Churyumov–Gerasimenko. The underlying inverse gas model is constructed by fitting ten thousands of measurements to thousands of potential gas sources distributed across the entire nucleus surface. The ensuing self-consistent solution for the entire coma density and surface activity reproduces the temporal and spatial variations seen in the data for monthly periods with Pearson correlation coefficients of 0.93 and higher. For different seasonal illumination conditions before and after perihelion, we observe a systematic shift of gas sources on the nucleus.

Key words: methods: analytical – methods: data analysis – methods: numerical – comets: general – comets: individual: 67P/Churyumov–Gerasimenko.

1 INTRODUCTION

The *Rosetta* mission provides a systematic study of the comet 67P/Churyumov–Gerasimenko (67P/C-G) on its way across the inner Solar system. In contrast to previous fly-by missions, *Rosetta* monitored the cometary environment constantly with a wide variety of instruments (Schulz 2009). The nucleus of comets consists of a mixture of dust and ice (Huebner et al. 2006). Upon approaching the inner Solar system, the nucleus heats up, frozen volatiles sublimate and gas together with dust is released. The continuous emission results in a coma, consisting of neutral and ionized species, and gives rise to a tail region surrounding the nucleus. Depending on the composition, size and activity of the nucleus, the gas and dust densities vary considerably. For 67P/C-G approaching the sun, the total gas production rate increased with peak activity occurring ∼20 d after perihelion (Hansen et al. 2016). The COmetary Pressure Sensor (COPS) on-board *Rosetta* has probed the gas density and dynamic pressure over a period of several months and thus provides a significant data set for a comet coma with a high temporal resolution in 1-min intervals (Balsiger et al. 2007). Due to the spreading and mixing of gas in space and the unknown surface emission rates, it is not possible to deduce from the *in situ* coma measurements directly the local surface activity at the sub-spacecraft points. The surface emission from different points on the nucleus is the input to any model of the entire coma (Combi, Harris & Smyth 2004). The deduction of surface properties from coma features requires to solve the inverse problem, which is formulated here as an optimization procedure. The complexity of the inversion is increased by the need of an accurate gas model and by the large amount of *in situ* data points. For instance, the direct simulations Monte Carlo (DSMC) method brings along most accurate atomistic results (Bird 1994), but cannot be applied to study all possible surface emission scenarios to be compared with the COPS data (Fougere et al. 2016). In addition, the complicated non-convex nucleus shape of 67P/C-G does not admit model reductions by symmetry considerations and further increases the computational complexity. Here, we present a different approach to describe the coma, which allows us to assimilate the large amount of measurements collected by COPS on board *Rosetta* at moderate computational costs. We carry out the inversion and optimization procedure to find the converged, self-consistent gas field and the corresponding distribution of surface emitters on 67P/C-G. To stay numerically efficient, we work with simplified gas equations and neglect collisions in the tenuous atmosphere around 67P/C-G. The converged source distribution minimizes the least-squares deviation of the measured versus modelled density at *Rosetta*'s position and reproduces the COPS data set over several weeks with high Pearson correlation coefficients of 0.93–0.99.

This paper is organized as follows: In Section 2, we describe the mathematical model and the optimization procedure, and in Section 3, we discuss the resulting gas emission from surface sources. We apply the model to different heliocentric distances of 67P/C-G and discuss the ensuing gas field for varying sub-solar latitudes, corresponding to pre-equinox (2015 April), equinox (2015 June), shortly after perihelion (2015 September) and 9 months past perihelion (2016 May) conditions. Finally, we describe how the gas sources are shifting with the changing seasonal solar

★ E-mail: kramer@zib.de

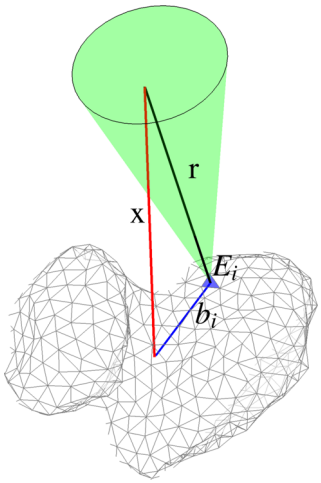

Figure 1. Low-resolution triangular-shape approximation $S^{(1024)}$ for the comet 67P/C-G and coordinate system for an exemplary gas source located at the highlighted triangular face E_i.

illumination along the orbit of 67P/C-G and how the sources correlate with optical *Rosetta* observations.

2 COMETARY GAS MODELS

A common ancestor of all cometary gas models is the Haser (1957) model for gas emitted constantly in time from a spherical nucleus and with a constant radial velocity. Neglecting ionization, the equation of continuity implies a x^{-2} drop of the neutral gas density with distance x from the comet. Other coma models consider more complex gas dynamics around a non-spherical nuclear shape. Here, we are considering the inner coma up to a distance of 400 km. Up to this distance, the gas distributes within ∼400 s, and retardation effects due to the rotation of the nucleus can be neglected. The gas density in this space increases from 10^{15} molecules m^{-3} in 2015 April (heliocentric distance 1.8 au) to 10^{18} molecules m^{-3} two weeks after perihelion (heliocentric distance 1.3 au). For the months excluding perihelion, this implies a relatively large mean free path length $l_{\rm mfp} = 5000$–50 m and Knudsen number $\mathrm{Kn} = l_{\rm mfp}/L = 0.1$–$10$, and indicates that collisions occur less frequently compared to more active comets, where $l'_{\rm mfp} = 0.1$–1 m (Gombosi, Nagy & Cravens 1986). The small amount of collisions allows us to build up a coma model from the analytical gas equations for the collisionless case (Narasimha 1962). The analytical gas solutions match the DSMC results for high Knudsen numbers $\mathrm{Kn} = l_{\rm mfp}/L \gg 1$ (Cai & Wang 2012), while at lower Knudsen numbers, $\mathrm{Kn} \sim 0.1$, the error is below 19 per cent. For the highest gas densities encountered in the weeks after perihelion, the collisionless approximation introduces a larger relative error of 0.18, but still fits the observations with a Pearson correlation 0.93; see Table 2.

2.1 Contribution of a single surface face

For the presented model, the shape of 67P/C-G with concave areas is approximated by a high-resolution triangular surface mesh. Each mesh face acts as a potential gas source, albeit with a position-dependent activity; see Fig. 1. The momentary gas density at the spacecraft position $\boldsymbol{x} \in \mathbb{R}^3$ results from the linear superposition of all visible gas sources, possibly located on different parts of the bi-lobed nucleus. As a consequence, the dominant factor for the variability in the gas density around 67P/C-G is the irregular shape of the nucleus. Let us assume a piecewise triangular shape approximation $S^{(n)}$ for the surface based on n triangular surface elements E_i, namely

$$S^{(n)} = \bigcup_{i=1}^{n} E_i .$$

Each face E_i emits collisionless gas into a surrounding vacuum with a point gas-source centred at $\boldsymbol{b}_i$ = center of mass(E_i) and pointing along the outward surface normal $\boldsymbol{v}_i$. For this case, Narasimha (1962) derives the analytical results for a gas temperature T and outflow velocity u_0. Introducing the parameter $\beta = 1/(2RT)$, with specific gas constant R and $U_0 = u_0\sqrt{\beta}$, the density profile at a space point $\boldsymbol{x} = \boldsymbol{b}_i + \boldsymbol{r}$ is given by

$$\rho_i(\boldsymbol{x}) = \begin{cases} \frac{U_0}{\pi}\frac{\cos\theta}{r^2}|E_i|q_i \exp(-U_0^2 \sin^2\theta), & \text{if } \cos\theta > 0 \\ 0, & \text{otherwise} \end{cases} . \quad (1)$$

Here, $r = |\boldsymbol{r}|$, $\cos\theta = \boldsymbol{r}\cdot\boldsymbol{v}_i/r$ and the source strength is denoted by q_i. With the corresponding velocity field,

$$\boldsymbol{u}_i(\boldsymbol{x}) = \frac{\boldsymbol{r}}{r}\frac{U_0}{\sqrt{\beta}}\cos(\theta), \quad \text{for} \quad \cos\theta > 0, \quad (2)$$

the momentum field becomes free of sources, i.e. $\mathrm{div}(\rho_i \boldsymbol{u}_i) = 0$. The momentum field carries along the molecular production rate $\dot{\rho}_i$ from a source on face E_i at any distance $\epsilon > 0$:

$$\dot{\rho}_i = \int_{\boldsymbol{r}\cdot\boldsymbol{v}_i=\epsilon} \rho_i \boldsymbol{u}_i \cdot \boldsymbol{v}_i \mathrm{d}\sigma = \left(1 - \frac{F(U_0)}{U_0}\right)\frac{|E_i|q_i}{\sqrt{\beta}}. \quad (3)$$

The factor $1 - F(U_0)/U_0$, with Dawson's integral F, approaches 1 for $1 < U_0$. In this limit, $|E_i|q_i/\sqrt{\beta}$ is the production rate $\dot{\rho}_i$, and

$$\dot{\rho}_{i,\rm surf} = \frac{q_i}{\sqrt{\beta}} \quad (4)$$

becomes the surface emission rate (flux) with the unit molecules per time and surface area. In general, the gas variables ρ_i and $\boldsymbol{u}_i$ are functions in space and time, and depend on the previously and momentary received solar radiation. We consider the time-averaged (over several weeks) surface emission rate and do not consider oscillations caused by the momentary illumination conditions. This restriction clearly brings out the spatial variations of the surface emission rate and does not introduce a large error in the description of each monthly COPS data set, as will be discussed in the following sections.

2.2 Construction of the entire gas coma

The gas emission of the complete shape $S^{(n)}$ is described by the linear superposition of all face contributions (1). The model builds on an accurate shape representation of the nucleus, given by a regular triangular surface mesh and including concave areas. We use a shape model with 9996 nearly equally sized triangles derived by uniform remeshing from the high-resolution model constructed by Malmer (2015). The bi-lobed shape and the concavities found on the surface of 67P/C-G require to consider the obstruction of gas sources according to the spacecraft location. Since the gas expands along straight lines (equation 2), a face E_i contributes only to an observation point $\boldsymbol{x} \in \mathbb{R}^3$ if the line between $\boldsymbol{b}_i$ and $\boldsymbol{x}$ does not cross the surface of the shape $S^{(n)}$. Summing up over all faces gives the gas density around the comet:

$$\rho(\boldsymbol{x}) = \sum_{i=1}^{n} \mathrm{occ}_i(\boldsymbol{x})\rho_i(\boldsymbol{x}), \quad \rho\boldsymbol{u}(\boldsymbol{x}) = \sum_{i=1}^{n} \mathrm{occ}_i(\boldsymbol{x})\rho_i\boldsymbol{u}_i(\boldsymbol{x}), \quad (5)$$

Table 1. Summary of the distance between *Rosetta* and comet, sub-solar latitude and heliocentric distance for all analysed months.

	Rosetta distance (km)	Sub-solar latitude	Heliocentric distance (au)
2015 April equinox	179–91	10.°4–4.°1	1.89–1.75
2015 May 11		0°	
2015 June perihelion	160–234	−9.°5 to −25.°3	1.52–1.35
2015 August 13		−47.°8	1.24
2015 August 22–September 18 summer solstice	312–442	−50.°8 to −52.°3	1.25–1.32
2015 September 5 equinox		−52.°3	1.28
2016 March 23		0°	
2016 May	7.1–18.6	5.°8–9.°6	2.91–3.12

$$\mathrm{occ}_i(\boldsymbol{x}) = \begin{cases} 0, & \text{if the line between } \boldsymbol{b}_i \text{ and } \boldsymbol{x} \text{ crosses } S^{(n)} \\ 1, & \text{otherwise} \end{cases}.$$

Neglecting any molecular desorption or adsorption, the total production rate Q of the comet shape $S^{(n)}$ arises from the sum of all source contributions. The outflow across a reference sphere of radius $R > 0$ and with surface element $\mathrm{d}\sigma$ is given by

$$Q = \int_{|\boldsymbol{x}|=R} \rho \boldsymbol{u} \cdot \boldsymbol{\nu} \, \mathrm{d}\sigma. \tag{6}$$

For the simplified case of a convex comet shape ($\mathrm{occ}_i = 1$), we obtain

$$Q_{\text{convex}} = \sum_{i=1}^{n} \dot{\rho}_i.$$

If we assume, in addition, a spatially homogeneous activity $\dot{\rho}_i = Q_0/n$ for all faces $i = 1, \ldots, n$, one recovers the Haser (1957) model with the total production rate given by

$$Q_{\text{Haser}} = 4\pi R^2 u_0 \rho(R) = Q_0.$$

For 67P/C-G, the last two simplifications do not seem appropriate and we use the general expression (6).

2.3 Parameter evaluation for the inverse gas model

The gas distribution in the coma depends on the parameters U_0 and q_i in (1), to be specified for all $i = 1, \ldots, n$ faces. The inverse problem consists of determining these $n + 1$ parameters by making use of the larger set of N measured gas densities ρ_j in the coma at different spatial positions $\boldsymbol{x}_j$:

$$(\boldsymbol{x}_j, \rho_j) \in \mathbb{R}^3 \times \mathbb{R}, \quad \text{for} \quad j = 1, \ldots, N.$$

For $n + 1 < N$, the system of equations relating the n faces to the N observations $\boldsymbol{\rho} = (\rho_1, \ldots, \rho_N)$ results in an overdetermined problem and is non-linear in U_0. Applying equation (5), we abbreviate this parametric dependence by

$$\rho_{U_0,\boldsymbol{q}}(\boldsymbol{x}_i) = \rho_i, \quad i = 1, \ldots, N$$

with respect to U_0 and the unknown surface activity parameters $\boldsymbol{q} = (q_1, \ldots, q_n)$. The problem statement is readily expressed in a matrix form by $M_{U_0}\boldsymbol{q} = \boldsymbol{\rho}$, with the model matrix $M_{U_0} \in \mathbb{R}^{n\times N}$ containing the contribution of every surface triangle to a given COPS location. We require $(U_0, \boldsymbol{q}) \in \mathbb{R}^{n+1}$ to give the minimal error between observation data and model:

$$\min_{(U_0', \boldsymbol{q}') \in \mathbb{R}^{n+1}} \| M_{U_0'}\boldsymbol{q}' - \boldsymbol{\rho} \|_{l^2(\mathbb{R}^N)}.$$

Having found this optimal solution set U_0 and $\boldsymbol{q}$, the gas field results from equation (5). The relative l^2-error for the optimal solution is given by

$$err = \frac{\| M_{U_0}\boldsymbol{q} - \boldsymbol{\rho} \|_{l^2(\mathbb{R}^N)}}{\| \boldsymbol{\rho} \|_{l^2(\mathbb{R}^N)}}. \tag{7}$$

The same inverse optimization procedure could be applied to other gas models. For the analytical gas model used here (equation 1), the matrix M_{U_0} is constructed very efficiently.

Table 2. Parameters for the gas model coupled to $n = 9996$ triangular faces to represent the shape of comet 67P/C-G.

Monthly data set	2015 April	2015 June	2015 September	2016 May
COPS samples (N)	21 125	32 860	32 710	24 817
Gas species	H_2O	H_2O	H_2O	CO_2
Pearson correlation	0.97	0.93	0.93	0.99
Error from equation (7)	0.12	0.18	0.18	0.11

3 OBSERVATIONAL DATA AND MODEL RESULTS

The model is evaluated directly at *Rosetta*'s sampling points and at a reference sphere with a radius of 100 km. Finally, we give the corresponding surface emission rate on the cometary surface. As input, we take the observational data of *Rosetta*'s COPS for four months in 2015 and 2016. COPS consists of two gauges. The Nude Gauge measures the total neutral gas density and the Ram Gauge

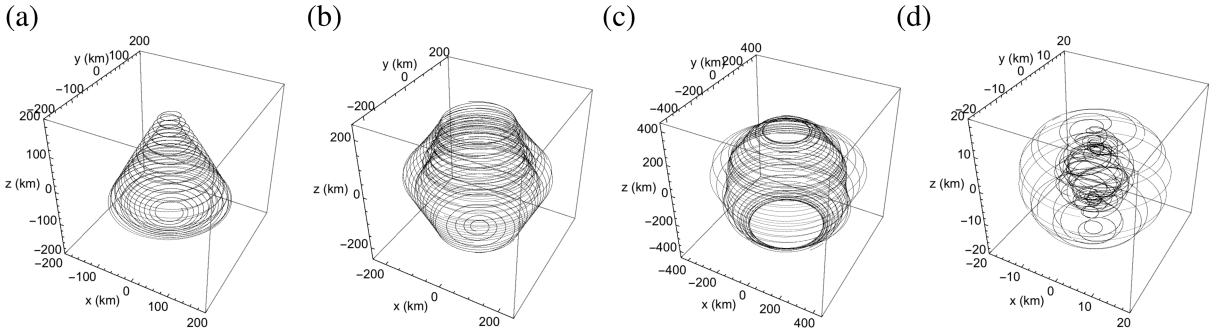

Figure 2. *Rosetta*'s orbit in the comet-fixed frame for the four COPS data sets considered: (a) 2015 April 12–31; (b) 2015 June; (c) 2015 September; and (d) 2016 May. In all cases, *Rosetta* surveys the entire surface of the nucleus, which rotates with a period of ∼12.4 h.

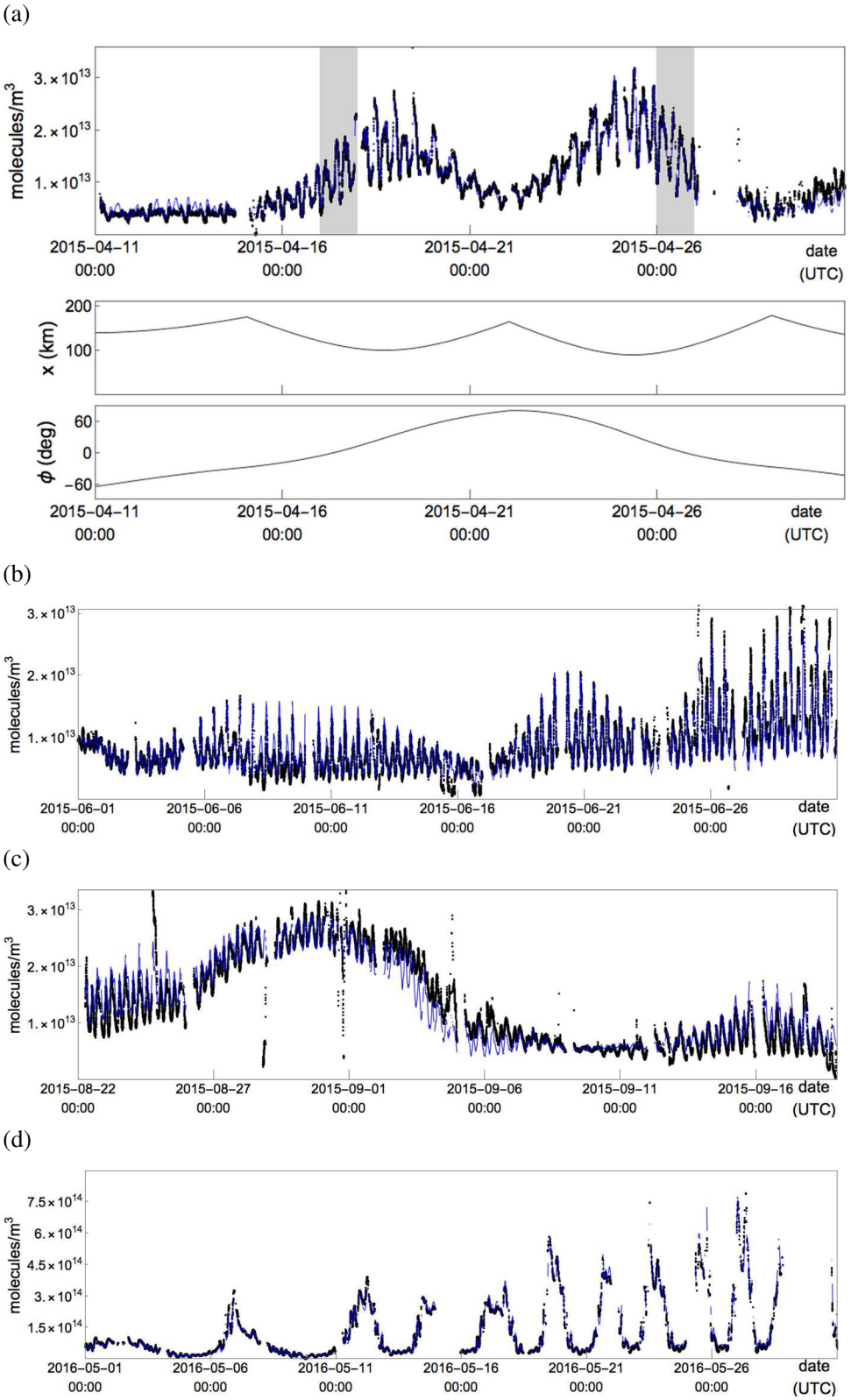

Figure 3. Modelled gas number density (blue lines) versus COPS data (black dots) for (a) 2015 April, (b) 2015 June, (c) 2015 September, and (d) 2016 May. Narrow spikes (instrument pointing and thruster operation related) in the COPS data have been removed. (a) The shaded time intervals are shown in detail in Fig. 7. The sub-panels display the distance x of *Rosetta* from the nucleus and the sub-spacecraft latitude ϕ.

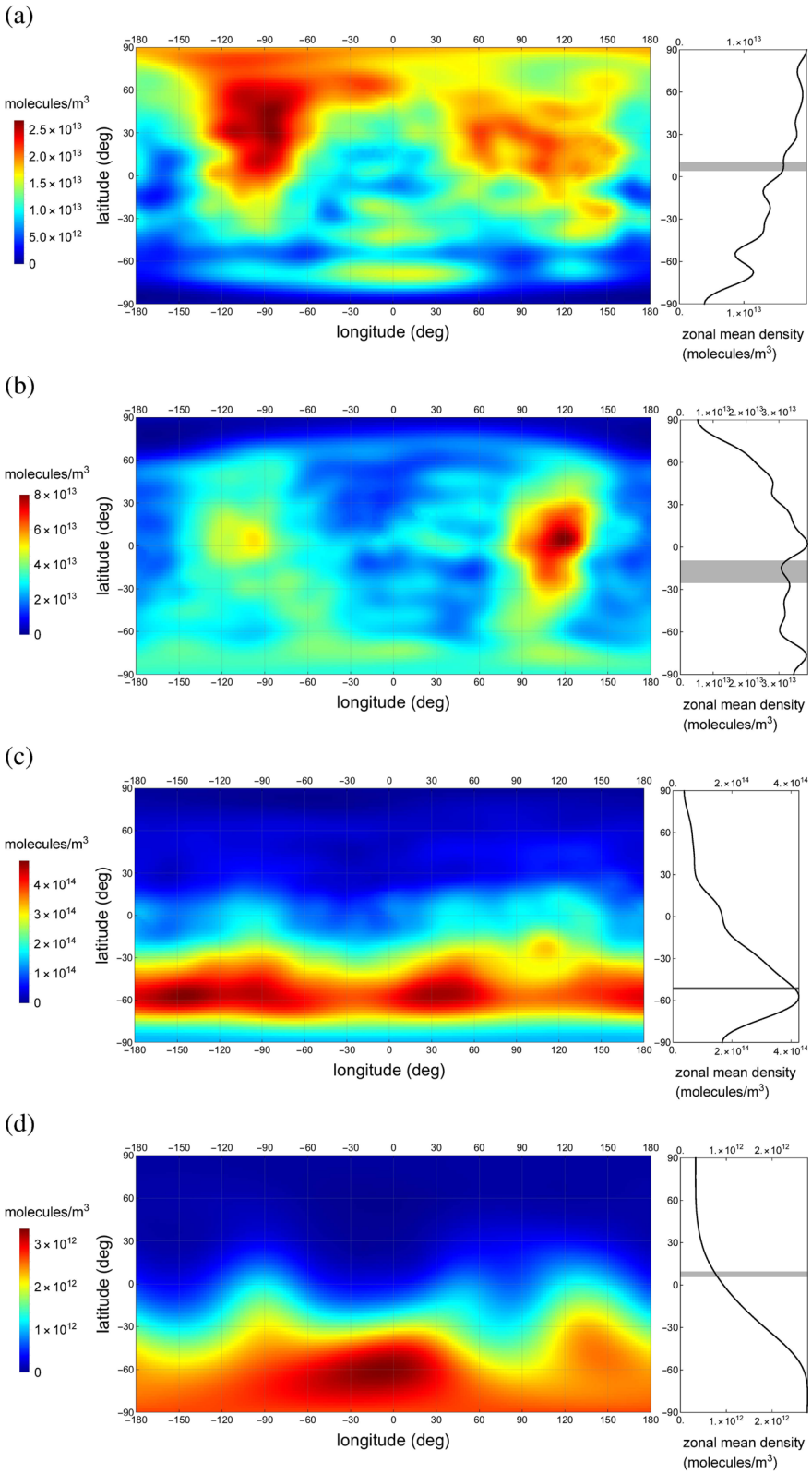

Figure 4. Model gas density at a distance of 100 km from the comet for (a) 2015 April, (b) 2015 June, (c) 2015 September, and (d) 2016 May. The side panels show the zonal mean density, and the grey bars denote the subsolar latitude during the observation time. The highest gas densities shift from the Northern to the Southern hemisphere.

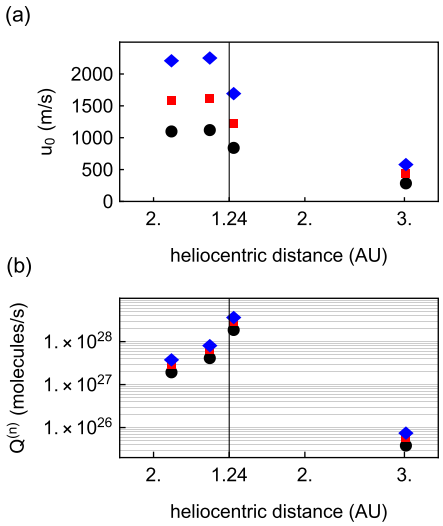

Figure 5. (a) Velocity u_0 leading to best agreement with COPS data and (b) total volatile emission rates for (from the left- to right-hand side) 2015 April, 2015 September 2015 June and 2016 May. The symbols denote three different coma temperatures: 50 (circle), 100 (square) and 200 K (diamond). The perihelion distance is marked by the vertical line.

records the dynamic pressure of the gas that emanates from the nucleus (Balsiger et al. 2007). For this work, COPS Nude gauge measurements are used. In the Nude Gauge, a hot filament emits electrons that are then accelerated towards the anode grid in which they ionize neutral particles. The resulting ions are measured with a sensitive electrometer. For the data set shown here, first the spacecraft background gas surrounding *Rosetta* (Schläppi et al. 2010) is subtracted to obtain the density of the cometary volatiles. COPS calibration in the laboratory has been performed with molecular nitrogen N_2. The measured densities at the comet have been corrected for different compositions to account for the species-dependent instrument sensitivities with respect to N_2. Around 67P/C-G, water vapour H_2O is the most abundant species besides CO and CO_2 at a larger heliocentric distance (Fougere et al. 2016). For simplicity, we assume a one-component coma, which introduces errors of the order of 10 per cent. On top of that, the errors in COPS absolute densities are approximately 15 per cent, yielding a total error of 18 per cent.

3.1 Inverse gas model for COPS data

We consider data sets for four distinct months: 2015 April, 2015 June, 2015 September and 2016 May. Each of the data set represents a characteristic phase of the cometary orbit with respect to sub-solar latitude; see Table 1. The inbound equinox occurs between the first two considered months, 2015 April and June, which are still before perihelion. The 2015 September set covers the highest activity period directly after perihelion. The last COPS data set from 2016 May surveys a period after outbound equinox and nine months after perihelion. For all observation months, *Rosetta* surveyed the entire nucleus with all surface areas within sight; see Fig. 2. For 2015 April and June, the distance from *Rosetta* to 67P/C-G is above 100 km; in 2015 September, it increases to 400 km; and for 2016 May, the distance stays below 20 km. All model results and least-square fits are performed for the shape model $S^{(n)}$ with $n = 9996$ and N COPS density measurements, summarized in Table 2. For all cases, the relative error equation (7) is in the range 0.11–0.18, which results in high Pearson correlation coefficients (0.93–0.99) between the measured data and the model. The high correlation coefficients show that the ansatz of a linear superposition of gas sources provides an accurate parametrization of the COPS data set, despite the assumption of a stationary and collisionless gas flow. The remaining differences between the inverse model and the observations stem from sporadic outbursts in gas emissions, instrumental uncertainties and gas collisions. In Fig. 3, we show a direct comparison of the measured number density and the model results from equation (5) for (a) 2015 April, (b) 2015 June, (c) 2015 September, and (d) 2016 May. The overall increase of the gas density around April 16–21 and 23–29 originates from the reduced distance of *Rosetta* from the nucleus (Fig. 3, second panel), while the daily variations reflect the distribution of gas sources on the nucleus.

3.2 Gas density at 100 km distance and on the surface

The COPS measurements provide a good sampling of the entire latitude/longitude range of the nucleus, but at varying radial distance (Fig. 2). The parametrization of the data set in terms of the gas model makes it possible to reconstruct the COPS data set on a spherical surface at a fixed distance of 100 km; see Fig. 4. The small error between the COPS data and the model during the entire monthly data set is an indication that the stationary approximation provides a suitable description of the emission process. A continuous gas release is reflected in similar, repetitive density variations along *Rosetta*'s orbit, which appear for similar *Rosetta*-nucleus viewing geometries (Fig. 7).

The 100-km densities show a three-fold increase of the absolute gas density towards perihelion from 3×10^{13} (2015 April) to 5×10^{14} m^{-3} shortly after perihelion (2015 September). In 2016 May, the maximum density drops to 3×10^{12} m^{-3}. In this month, the emitted gas is taken to be CO_2. The seasonal effects are shown in the zonal mean densities (lateral panels in Fig. 4), which undergo a systematic shift of highest densities from northern to southern latitudes. One month before equinox (2015 April), the peak zonal density stems from two areas at (longitude, latitude) $= (-90^\circ, 45^\circ)$ and $(100^\circ, 20^\circ)$. Both areas are still visible in 2015 June and show increased densities of 5×10^{13} and 8×10^{13} m^{-3}, respectively. Summer solstice (2015 September 5) follows 23 d after perihelion. Around this time, the Southern hemisphere received the largest solar radiation, and the zonal density in 2015 September attains its highest value at the corresponding sub-solar latitudes; see Fig. 4(c). In the other months, the maxima in the zonal mean density are not occurring at the mean sub-solar latitude during the corresponding observation month, indicated by the bars in the zonal panels. In particular, CO_2 sources in the Southern hemisphere are still present in the zonal density distribution for 2016 May (Fig. 4d), long after perihelion and after outbound equinox, which puts the sub-solar latitude to the Northern hemisphere.

3.3 Total and surface emission rates

The gas model in Section 2, together with the fit to the COPS data in Section 3.1, allows us to obtain the outflow velocity u_0, the surface emission rates $\dot{\rho}_{i,\mathrm{surf}}$ and the total production rate Q. The fit to the COPS densities in Section 2.3 yields the best value for the parameter U_0, but does not set the absolute value of the coma gas velocity u_0. To obtain emission rates requires to specify the velocity field equation (2), which includes the parameter β and, through it, the

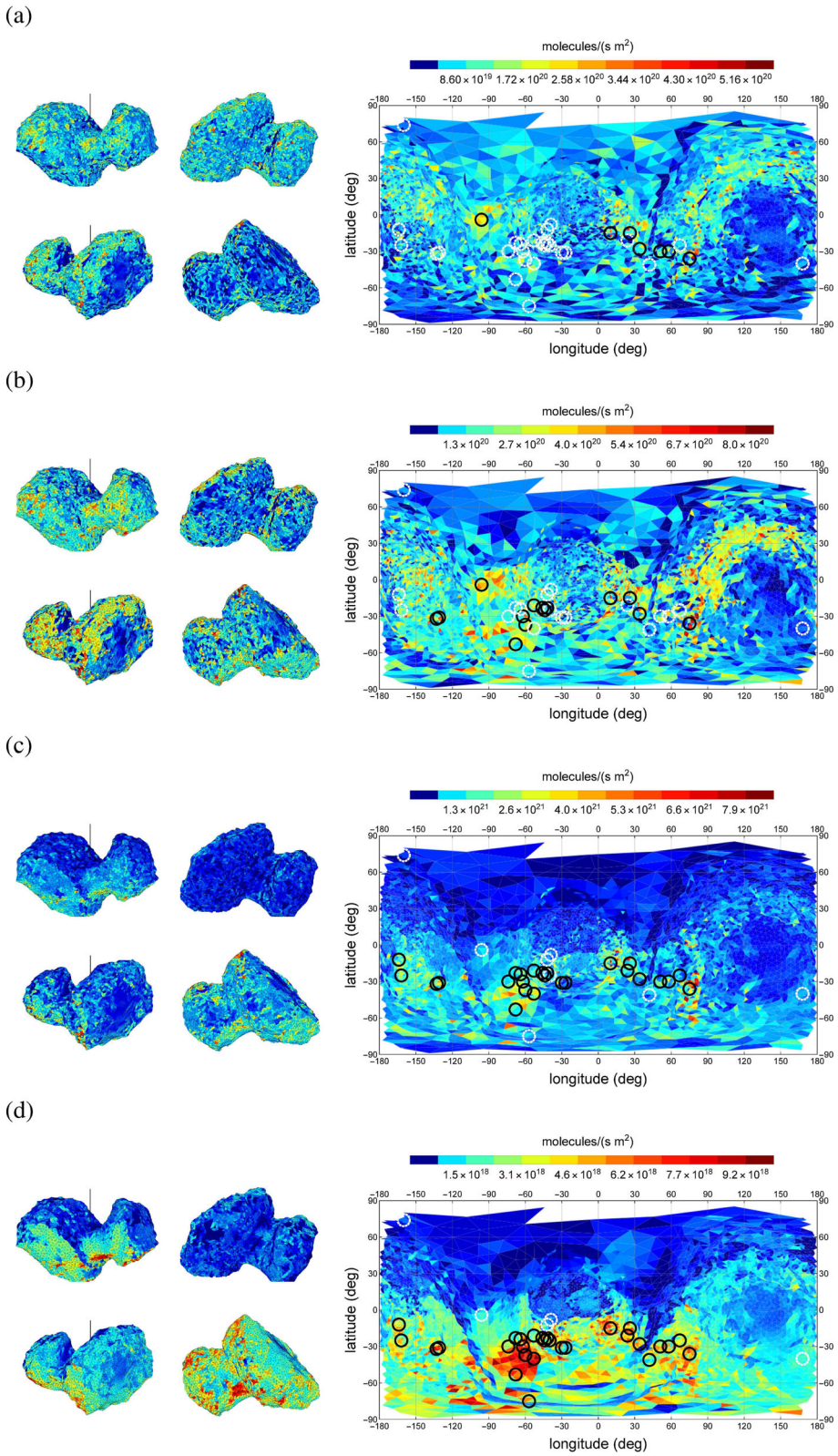

Figure 6. Surface gas emission rates for (a) 2015 April, (b) 2015 June (c) 2015 September and (d) 2016 May originating from the inverse gas model for the COPS data set. In the left-hand panels, the different 3D views include the rotational axis. In the right-hand panels, a global map is shown. In addition to the general migration of gas sources from northern parts to the southern parts, more localized gas source regions are revealed. The circles indicate locations of dust outbursts during perihelion reported by Vincent et al. (2016). Solid black circle: correlation between dust outbursts and gas-emitting areas; dotted white circle: no correlation.

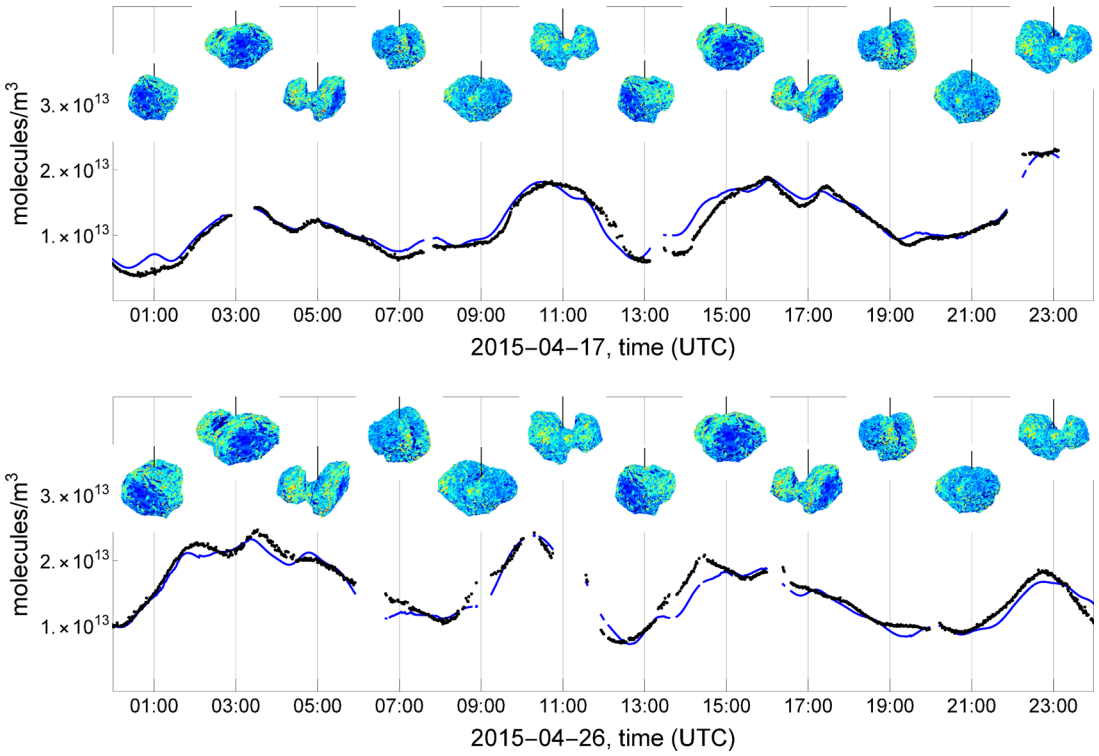

Figure 7. Diurnal variation of the gas density for two different days (2015 April 17 and 26); COPS data are marked by black dots and the blue line shows the modelled gas density. The inset shows the momentary view from *Rosetta*'s orbital position. *Rosetta* surveys similar surface areas on both days, and the gas densities show a repetitive pattern. This indicates spatial and temporal permanence of the gas sources.

coma gas temperature T. According to Gombosi et al. (1986), Biver et al. (2015), Rubin et al. (2014) and Huang et al. (2016), adiabatic cooling of the gas during expansion into vacuum leads to a reduction in gas temperature compared to the surface temperature. We study the parameter sensitivity by considering three different temperatures $T = 50$, 100 and 200 K. The resulting range of outflow velocities u_0 and total production rates Q is shown in Fig. 5. The total production rate increases towards perihelion and reaches 2.0×10^{28}–4.0×10^{28} molecules s^{-1} shortly after perihelion (2015 September). The values obtained here are within the ranges shown in fig. 9 of Hansen et al. (2016). In 2016 May, the total production rate has dropped to $(4.1–8.1) \times 10^{25}$ molecules s^{-1}. Besides the total production rate, the gas model underlying the COPS fit determines the local surface emission rates with a high spatial resolution. For the case of a coma gas temperature of $T = 100$ K, the corresponding surface emission is shown in Fig. 6 according to equation (4). Similar surface regions are active in 2015 April and June. The two density maxima described in Figs 4(a) and (b) may be attributed to widespread gas sources around (longitude, latitude) = (−90°, 0°) (Anuket region) and (60° to 90°, 0° to −45°) (Aten and Khepry regions). The overall drift of the density maxima from north to south in Fig. 4 is reflected in the changes of the emission rates. Directly after perihelion in 2015 September, the water emission from the surface resembles the illumination conditions during that time (see fig. 2 in Lai et al. 2016). Several months later (2016 May), the surface emission comes from the Southern hemisphere (Fig. 6d), and shows the decoupling of the CO_2 gas production from the sub-solar latitude at that time; see Table 1. The same localized source regions are observed for 2015 September and 2016 May around (−60°, −30° to −45°), at (10°, −15°) and at (75°, −40°). After perihelion, we find a correlation of more active gas-emitting areas (flux exceeds 3.5 times the average gas flux) with the locations of previous short (less than 5 min) dust outbursts observed optically around perihelion (Vincent et al. 2016), marked by black circles in all surface maps. In each of the two months, 2015 September and 2016 May, 29 out of 34 reported dust outburst locations are close to active gas emitters, while in 2015 June only 8 and in 2015 April 15 locations match. This observational correlation might indicate a persistence of CO_2 sources at dust outburst locations over nine months.

To illustrate how the surface sources are leading to specific COPS densities, Fig. 7 shows two periods of 24 h for COPS data and the modelled density. These periods are separated by 9 d in 2015 April and characterize similar overflight positions for *Rosetta*; see Fig. 3 for the complete data set. For both days, the gas densities give repetitive patterns for succeeding relative minima and maxima. The differences of magnitude are mostly related to slightly different *Rosetta* distances and are equivalent to a x^{-2} drop in the coma. These patterns show that the model assumption of time-independent but spatially varying surface emission rates results in a good agreement with the temporally varying COPS data.

4 SUMMARY

Within this paper, we have presented an inverse gas model approach for COPS data measurements around the comet 67P/C-G. The least-squares analysis leads to a solution for the given shape and set of observations. Coupled with the numerically efficient evaluation of the gas model, it reconstructs the COPS data spanning several weeks from a spatially varying surface emission map. The total production rates are in agreement with the combined ground observation and *Rosetta* data (Hansen et al. 2016). The surface maps support the hypothesis of a widespread gas release across the surface in

combination with additional localized gas sources. Localized source regions are consistently retrieved by the inverse model over distinct data sets separated by more than nine months. A similar model has been applied to describe the dust emission of 67P/C-G, with a similar correlation (>0.9) between optical dust observations and theoretical prediction (Kramer et al. 2015; Kramer & Noack 2016). Comparing different seasonal conditions before and after perihelion, we observe a systematic southward migration of the gas sources. In particular, several months after perihelion, the gas sources and the sub-solar latitude are not coinciding. This points to a north–south dichotomy with respect to the gas release.

ACKNOWLEDGEMENTS

The work was supported by the North-German Supercomputing Alliance (HLRN). We thank M. Malmer for helpful discussions. *Rosetta* is an ESA mission with contributions from its member states and NASA. We acknowledge herewith the work of the whole ESA Rosetta team. Work on ROSINA COPS at the University of Bern was funded by the State of Bern, the Swiss National Science Foundation and the European Space Agency PRODEX programme.

REFERENCES

Balsiger H. et al., 2007, Space Sci. Rev., 128, 745
Bird G. A., 1994, Molecular Gas Dynamics and the Direct Simulation of Gas Flows. Clarendon Press, Oxford
Biver N. et al., 2015, A&A, 583, A3
Cai C., Wang L., 2012, Theor. Appl. Mech., 2, L012004
Combi M. R., Harris W. M., Smyth W. H., 2004, in Festou M. C., Keller H. U., Weaver H. A., eds, Comets II. Univ. Arizona Press, Tucson, AZ, p. 523
Fougere N. et al., 2016, A&A, 588, A134
Gombosi T. I., Nagy A. F., Cravens T. E., 1986, Rev. Geophys., 24, 667
Hansen K. C. et al., 2016, MNRAS, 462, S491
Haser L., 1957, Bull. Class Sci. l'Académie R. Belg., 43, 740
Huang Z. et al., 2016, J. Geophys. Res., 121, 4247
Huebner W., Benkhoff J., Capria M.-T. A. C., De Sanctis C., Orosei R., Prialnik D., 2006, Heat and Gas Diffusion in Comet Nuclei. The International Space Science Institute, Bern
Kramer T., Noack M., 2016, AJ, 823, L11
Kramer T., Noack M., Baum D., Hege H.-C., Heller E. J., 2015, preprint (arXiv:1505.08041)
Lai I.-L. et al., 2016, MNRAS, 462, S533
Malmer M., 2015. Available at: http://mattias.malmer.nu/67pc-g-shape model/
Narasimha R., 1962, J. Fluid Mech., 12, 294
Rubin M. et al., 2014, AJ, 781, 86
Schläppi B. et al., 2010, J. Geophys. Res., 115, A12313
Schulz R., 2009, Sol. Syst. Res., 43, 343
Vincent J.-B. et al., 2016, MNRAS, 462, S184

This paper has been typeset from a TEX/LATEX file prepared by the author.